Single layer In-O atomic sheets as phonon and electron barriers in ZnO-In_2O_3 natural superlattices: Implications for thermoelectricity

Xin Liang, and David R. Clarke

Citation: Journal of Applied Physics **124**, 025101 (2018); doi: 10.1063/1.5027625
View online: https://doi.org/10.1063/1.5027625
View Table of Contents: http://aip.scitation.org/toc/jap/124/2
Published by the American Institute of Physics

Single layer In-O atomic sheets as phonon and electron barriers in ZnO-In_2O_3 natural superlattices: Implications for thermoelectricity

Xin Liang[a] and David R. Clarke
School of Engineering and Applied Sciences, Harvard University, Cambridge, Massachusetts 02138, USA

(Received 4 March 2018; accepted 18 June 2018; published online 11 July 2018)

The phases in the ZnO half of the ZnO-In_2O_3 binary system are natural superlattices consisting of a periodic stacking of single InO_2 sheets separated by indium doped ZnO blocks with a spacing that depends on the composition according to the relationship $In_2O_3(ZnO)_k$. Characterization by combined, atomic resolution, aberration-corrected scanning transmission electron microscopy and electron energy loss spectroscopy analysis indicates that the atomic structure of each InO_2 layer consists of a single continuous sheet of octahedrally coordinated InO_2. The sheets are also crystallographic inversion boundaries. Analysis of the electrical conductivity, thermal conductivity, and Seebeck coefficient data at 800 °C indicates that the InO_2 sheets not only decrease thermal conductivity by phonon scattering but also create potential barriers to electron transport. The origin of the potential barriers, the role of piezoelectric effects, and their dependence on superlattice spacing are discussed qualitatively. It is also argued that the crystallographically aligned InO_2 sheets within individual grains are also transport barriers in randomly oriented polycrystalline materials. *Published by AIP Publishing*. https://doi.org/10.1063/1.5027625

I. INTRODUCTION

Nanostructure engineering has been exploited in recent years to create thermoelectric materials with high figures of merit. This approach, which has included decreasing the grain size of polycrystalline materials, has arguably been most effective in semiconductor superlattice structures[1–4] and can be attributed to the high density of coherent interfaces that are effective in scattering phonons, dramatically decreasing thermal conductivity, while also modifying the density of states at the Fermi level to produce an increase in the Seebeck coefficient.[5] These superlattices as well as the crystallographically incoherent superlattices, such as W/alumina, that exhibit very low thermal conductivities[6–8] are all produced layer-by-layer, for instance, by molecular beam epitaxy (MBE).[6,9] Furthermore, synthetic superlattice structures are intrinsically morphologically unstable at high temperatures due to their high interfacial energy,[7,9] making them unsuitable for prolonged, high temperature applications.

A number of oxide semiconductors form superlattices naturally. These include $In_2O_3(ZnO)_k$,[10–17] $CaO(CaMnO_3)_k$,[18,19] $Na_xCo_2O_4$,[20,21] and $Ga_2O_3(ZnO)_k$,[22–24] where the integer k denotes the order of the superlattice structure. In the ZnO-based superlattices, the integer k describes the number of ZnO planes between the indium oxide layers[13,17,25] measured along the c-axis of the ZnO. The superlattices in these materials form from about 10 mol. % (m/o) to 40 m/o $InO_{1.5}$.[13,17] As they self-assemble on annealing at high temperatures, they can be made in bulk by sintering powders of the appropriate composition with their superlattice spacing determined directly by their overall composition. (For compositions less than about 10 m/o $InO_{1.5}$, individual indium ions dissolve into the ZnO blocks substituting for the Zn^{2+} ions. Such solid solution appears to entropically favored and is responsible for the observed increase in n-type electrical conductivity of ZnO when doped with In^{3+} ions. Similarly, compositions greater than 40 m/o $InO_{1.5}$ evolve into a two-phase system consisting of a mixture of In_2O_3 and a natural superlattice. The properties of these two-phase materials will not be discussed here since the In_2O_3 phase can act as a parallel conducting path, both electrically and thermally.) As the compounds are thermodynamically stable, the superlattices are, unlike grain or precipitate microstructures, resistant to coarsening at high temperatures[26] and remain morphologically stable.[17]

In this publication, we provide a detailed atomic structure of the superlattice interface, present data derived from the Seebeck coefficient on the electron barrier heights of the interfaces as a function of composition across the ZnO-In_2O_3 phase diagram, and relate them to the thermoelectric figure of merit previously reported for different superlattice compositions. The property data presented are for 800 °C in air as we are interested in high temperature thermoelectrics. Also, although these materials do not exhibit remarkable values of the figure of merit, it is anticipated that the systematic variation in properties with superlattice spacing presented in this work may nevertheless provide new insights.

II. EXPERIMENTAL DETAILS

ZnO-In_2O_3 powders having different indium oxide concentrations were synthesized using combined wet chemistry and gel combustion methods and then sintered into solid pellets using a current-assisted densification processing technique.[17,26] The materials made this way are bulk, randomly oriented, polycrystalline materials with a grain size of several microns.[17,26,27] Post-annealing treatments at 1250 °C for seven days were then given to the materials to stabilize the

[a]Present address: School of Materials Science and Engineering, Changzhou University, Jiangsu 213164, China.

superlattice spacings. At this temperature, the phase diagram and the superlattices are well documented. Thermal conductivity measurements were made using the laser flash method up to 1000 °C. Measurements of the electrical conductivities and Seebeck coefficient were made using a ULVAC RIKO ZEM 3 M10 unit. Complementary measurements from room temperature up to 800 °C have previously been reported.[17,26,27]

III. ATOMIC STRUCTURE OF THE SUPERLATTICE INTERFACE

Since their discovery, there has been some ambiguity as to the detailed atomic structure of the superlattice interfaces in the $In_2O_3(ZnO)_k$ system. Early on, the atomic structure was described as consisting of alternating, periodic stacking of blocks of In_2O_3 and k-unit cells of ZnO.[10] More recently, the atomic structure of these superlattice compounds has been revised and is now described as consisting of a periodic arrangement of a single, octahedrally coordinated InO_2 layer separating $(k+1)$ unit cells of ZnO stacked along the ZnO [0001] c-axis. This has been substantiated by crystal structure refinement[28] and by some high-resolution electron microscopy observations[14,29,30] as well as 3D atom probe tomography.[26] In this study, the atomic structure is unambiguously resolved as a single InO_2 layer using the atomic resolution aberration-corrected scanning transmission electron microscopy (STEM) angular dark field (ADF) imaging mode in a Hitachi HD-2700 microscope operating at 200 keV. An example is shown in Fig. 1(a) where the InO_2 sheets arranged in between blocks of ZnO are seen edge-on in a 10 m/o $InO_{1.5}$ doped ZnO post-annealed at 1250 °C for 7 days. In the ADF imaging mode, indium, having higher atomic mass, Z, than zinc, appears significantly brighter. Oxygen ions are not seen due to their much smaller atomic mass. (In ADF imaging, the contrast varies as Z-squared.) The atomic structure observed using aberration corrected STEM imaging confirms the atomic models determined by X-ray diffraction[25,31,32] and recent microscope based spectroscopy work by Schmid *et al.*[29,30] These studies show that the cation sites in the $In_2O_3(ZnO)_k$ superlattice interface are solely occupied by indium ions that sit on octahedral sites coordinated to oxygen ions. The localization of the indium ions is confirmed by electron energy loss spectroscopy (EELS) spectra recorded from adjacent atomic positions, one on the bright column of atoms and the other on the adjacent weak column of atoms, shown in Figs. 1(b) and 1(c), respectively. The spectrum recorded from a bright atom clearly reveals that it is In and O by the presence of the characteristic In-$M_{4,5}$, In-M_3, and O-K edges. The other spectrum recorded from an adjacent atomic position located off the InO_2 sheet has no discernable edges from Indium and only the Zn-$L_{2,3}$ and Zn-L_1 edges from the Zn in addition to the O-K edge. These measurements were confirmed by EELS spectra from successive atom positions across the InO_2 sheet, as shown in Fig. 2.

Crystallographically, the InO_2 sheets comprising the superlattice interface are coherent, inversion domain boundaries (IDBs) with the polar direction of the ZnO reversing across the boundary.[14,33] This is seen in the atomic model of Fig. 3 for the k = 6 composition constructed using a VESTA program[34] with the input of atomic coordinate information from a ICSD incorporated ICDD database.[35] Although the atomic arrangement for the $In_2O_3(ZnO)_6$ compound is shown

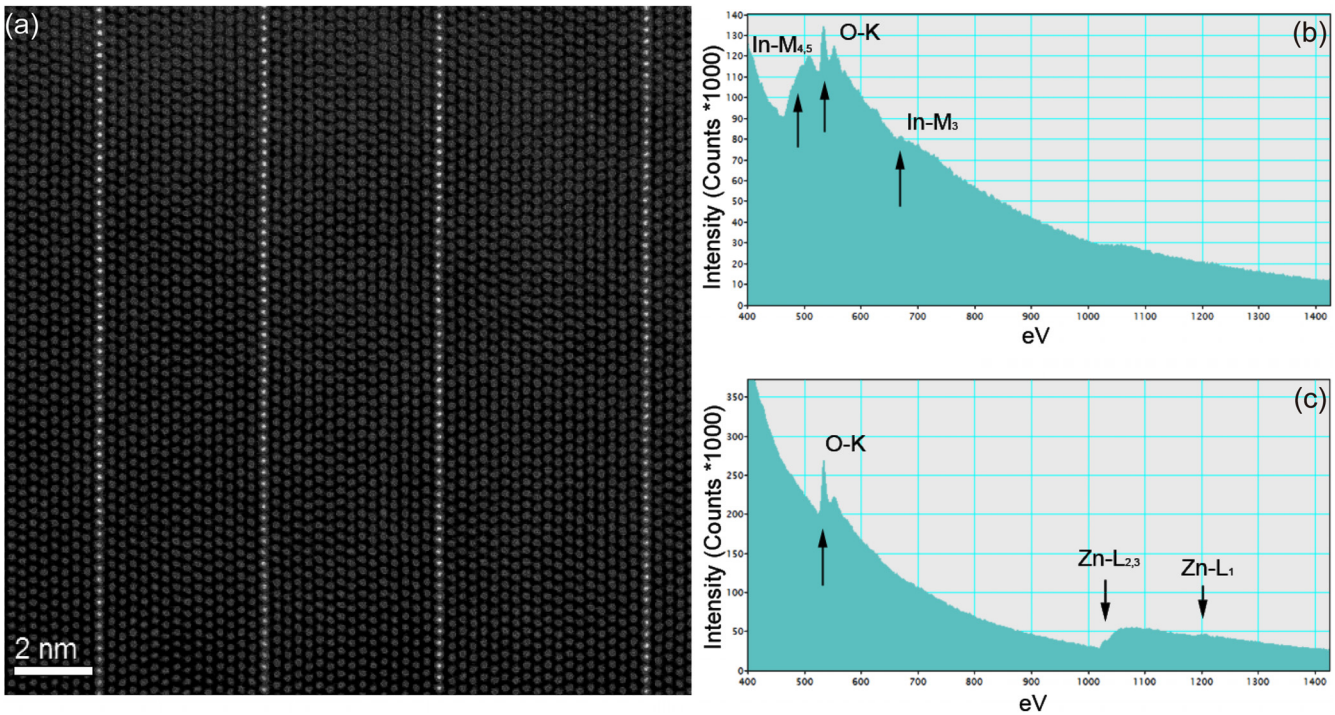

FIG. 1. (a) Aberration corrected STEM ADF image of $In_2O_3(ZnO)_k$ natural superlattice structure showing the InO_2 sheets end-on and perpendicular to the c-axis of the ZnO. (b) EELS spectra from one of the bright columns of atoms and (c) an adjacent atom column together showing that the Indium ions are localized in the bright sheets in (a). In common with all the other materials in this work, this sample was annealed at 1250 °C for 7 days. This particular superlattice image is chosen as it indicates that there can be local variations in the superlattice spacing.

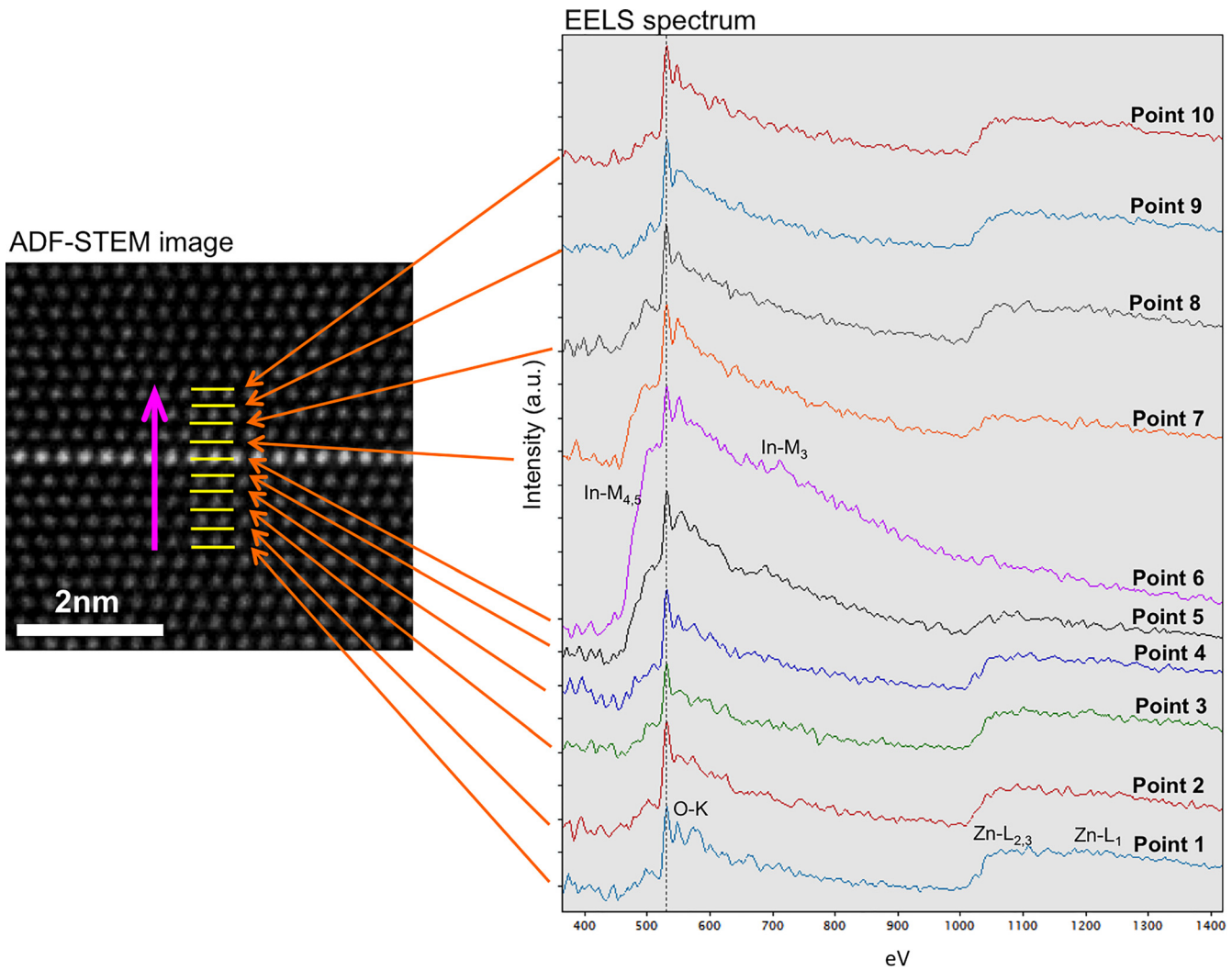

FIG. 2. Atomic resolution electron energy loss spectra recorded at successive atomic positions across the one of the bright rows of atoms in Fig. 1(a). These spectra provide further confirmation that the Indium ions are indeed localized to the bright sheets imaged edge on as suggested by other TEM images and by the X-ray diffraction in the literature.

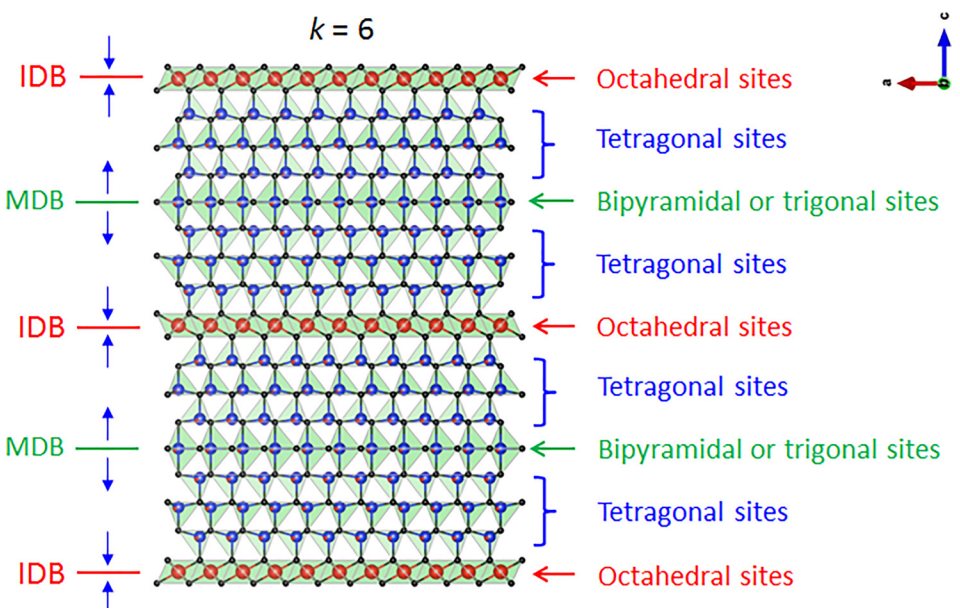

FIG. 3. Atomic model of the $In_2O_3(ZnO)_6$ superlattice compound viewed along the *b*-axis. Indium, zinc, and oxygen ions are represented by red, blue, and black circles, respectively. The In-O and Zn-O bondings are visualized by the superimposed polyhedra. On the right side of the model, cation occupation sites are indicated; on the left side, IDBs and MDBs are indicated and the direction of the positive c-axis vector in each ZnO block is represented by the blue arrow.

in this figure for illustration, all the superlattices, irrespective of their k value, consist of $(k+1)$ ZnO layers separating individual single-layer InO_2 sheets. Half-way between the InO_2 sheets and parallel to them is a mirror domain boundary (MDB) in the ZnO where there is a single sheet of zinc atoms with trigonal coordinated with five neighboring oxygen ions rather than the usual tetrahedral coordination.[28] Sometimes referred to as a plane of bipyramidal sites since this describes the local atomic coordination, there is again a reversal of the polar direction in the ZnO across this mirror plane.[30,36] According to the structure, this corresponds to a "tail-to-tail" change in polarity in the ZnO. The atomic structure of the superlattice in Fig. 3 is confirmed by the STEM ADF image with image matching. This confirms that there is a reversal in polarity in the ZnO at the InO_2 layer and also one at the mid-plane. Although the ideal structure consists of a single periodicity of the InO_2 sheets throughout the bulk materials, our observations indicate that there is always some variability in the spacing from region to region, even within individual grains, suggesting that compositional homogeneity and thermodynamic equilibrium were not completely attained. Within the majority of grains, all the superlattices are parallel to one another. Sub-grains occasionally form and within those, the superlattices are parallel to one another. In addition to this structural description of the superlattice, individual indium ions can also dissolve into the ZnO blocks substituting for the Zn^{2+} ions and enhancing the electrical conductivity.

IV. PHONON SCATTERING

As shown in Fig. 4, the thermal conductivity at 800 °C is dramatically reduced once sufficient In_2O_3 is alloyed into pure ZnO to form superlattices.[17,26,27] Indeed, at concentrations, above about 10 m/o $InO_{1.5}$, the thermal conductivity is almost independent of In_2O_3 concentration, having a value of ~2 W/m K, until In_2O_3 forms as a second phase at compositions above 40 m/o $InO_{1.5}$. Previous analysis of the thermal conductivity data as a function of superlattice spacing indicates that each InO_2 superlattice sheet has a thermal resistance, R_k, of $5.0\pm0.6\times10^{-10}\,m^2\,K/W$ at temperatures above room temperature.[26] This value of thermal resistance is intermediate between those reported for epitaxial semiconductor interfaces ($\sim10^{-10}$ m^2 K/W)[37] and those for grain boundaries ($10–50\times10^{-10}$ m^2 K/W).[38,39] The net thermal resistance perpendicular to the superlattice is then simply the sum of the thermal resistance of the In-doped ZnO blocks and the number of superlattice sheets in the unit length: $\frac{1}{\kappa}=\frac{1}{\kappa_{ZnO}}+\frac{R_k}{(k+1)d_{\{0002\}}}$. The origin of the thermal resistance is attributed to both the lattice distortions associated with the crystallographic inversion across the interface and also the significantly higher atomic mass of Indium (114.82 versus 65.38 for the mass of Zn). The grain size of the materials studied was several microns, far larger than the superlattice spacing, and so the thermal resistance of the grain boundaries can be neglected.

One explanation for the low and compositional independence of the thermal conductivity is that the superlattice causes zone folding, restricting the acoustic velocity. Direct evidence for zone folding by the superlattice structure comes from Raman and vibrational studies of materials across the ZnO-In_2O_3 phase diagram.[40] Over the compositional range at which the superlattices form, low energy Raman bands appear. Furthermore, their Raman shifts correspond to those expected based on zone folding of the acoustic modes along the c-axis of the ZnO, as shown in Fig. 5 taken from Ref. 40. In the same superlattice compositional range, new vibrational modes also appear and there is no evidence for the Raman modes of either ZnO or In_2O_3, the terminal phases of the binary phase diagram.

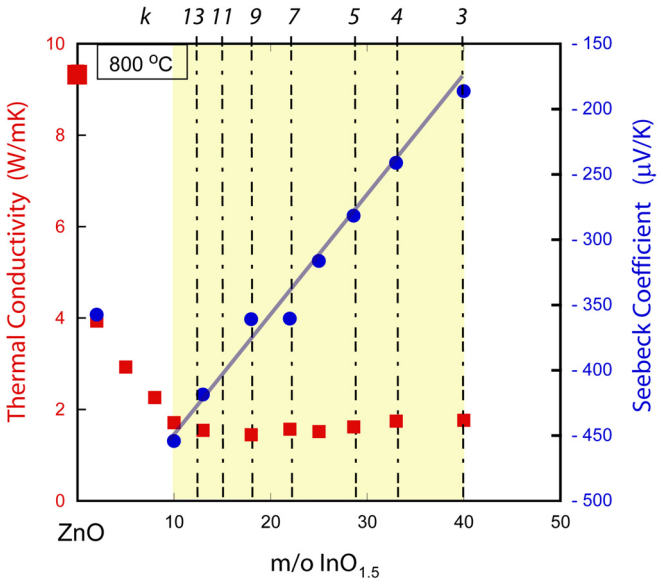

FIG. 4. Variation of thermal conductivity (red squares) and Seebeck coefficient with the indium oxide concentration, all at 800 °C, over the compositional range where natural $In_2O_3(ZnO)_k$ superlattices form (shaded). The k values corresponding to the compositions are labeled along the top axis. The line through the Seebeck coefficient data is a guide to the eye. In this and subsequent graphs, the composition is expressed in terms of constant cation concentration, $InO_{1.5}$ rather than In_2O_3.

V. ELECTRICAL CONDUCTIVITY AND SEEBECK COEFFICIENT

Over the compositional range that superlattices are observed to form, the electrical conductivity is almost independent of temperature from room temperature to 800 °C, as shown in Fig. 6. This is in marked contrast to the usual thermally activated electrical conductivity of semiconductors exhibited, for instance, in lightly doped ZnO doped with less than 0.03 a/o Al[41,42] or, for instance, with other solid solution dopants. The temperature independence is also not observed in our materials for doping below 10 m/o $InO_{1.5}$. Despite the temperature independence, the conductivity is observed to increase with the $InO_{1.5}$ concentration (Fig. 7) as might be expected, but whether this is due to an increase in overall doping alone or due to increases in mobility would require high-temperature Hall measurements. Conductivity increases are also not observed in polycrystalline ZnO-based varistors, which have cobalt-solid solution doping, and large ions, such as Bi and Pr, segregated to their grain boundaries. Consequently, this is believed to be a characteristic of

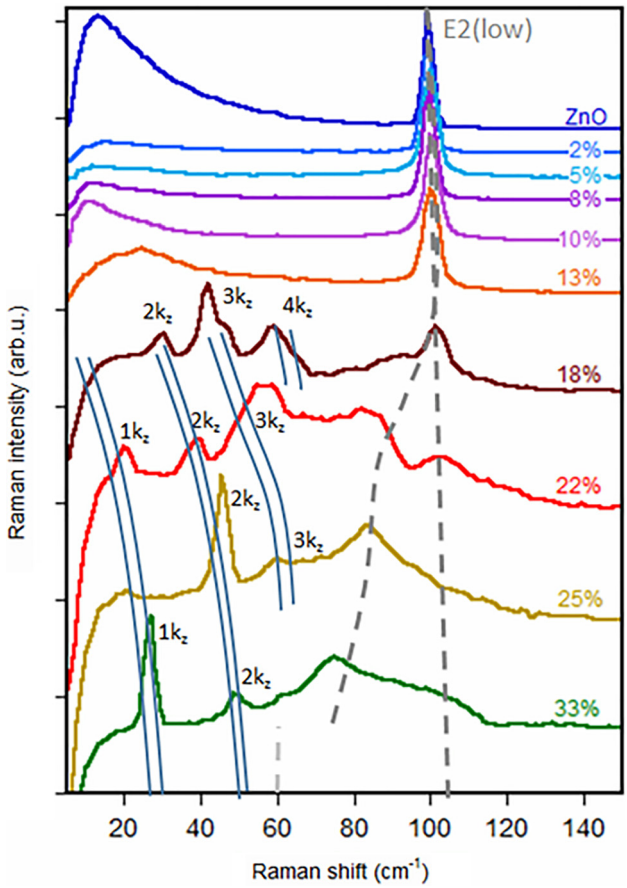

FIG. 5. Low frequency Raman spectra for the compositions indicated. The Raman modes associated with zone folding of the acoustic branch of the superlattices along the c-axis are labeled and compared with calculated folding (the continuous curves nk_z). Reproduced with permission from Margueron *et al.*, J. Appl. Phys. **119**, 195103 (2016). Copyright 2016 AIP Publishing LLC.[40]

electrical transport in these polycrystalline superlattice materials. Temperature-independent electrical conductivity is also one of the signature characteristics of tunneling controlled conductivity although we are unable to demonstrate experimentally that this is the case in these materials.

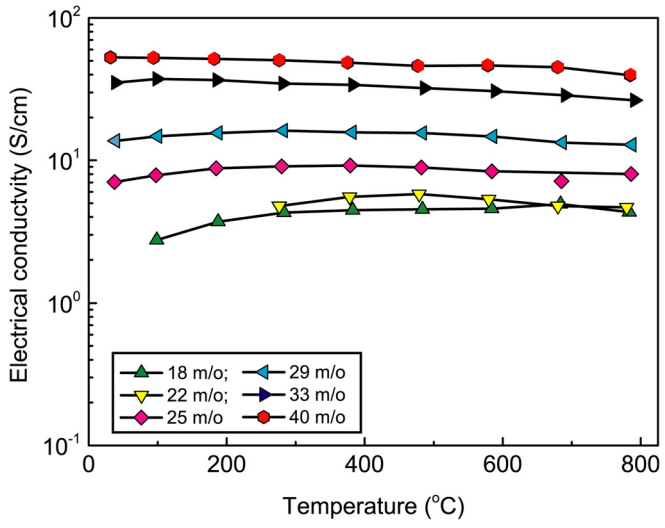

FIG. 6. The electrical conductivity of each of the natural superlattice structures is almost independent of temperature above room temperature.

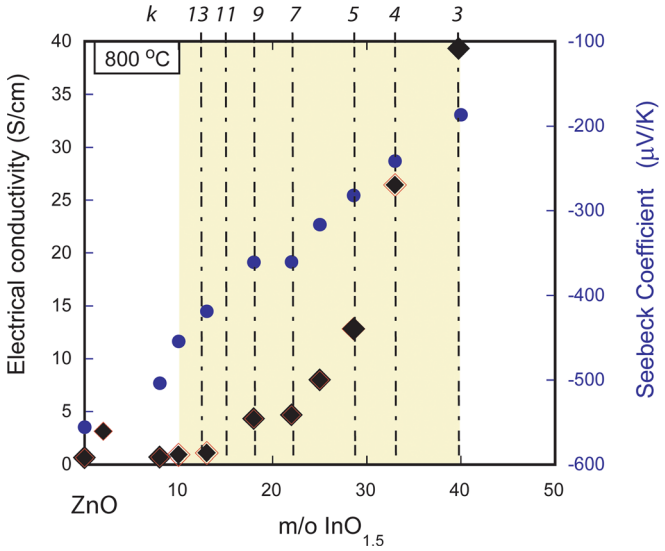

FIG. 7. Variation of electrical conductivity (black diamonds) and Seebeck coefficient (blue circles) at 800 °C over the compositional range that natural superlattices form.

Measurements of the Seebeck coefficient at 800 °C over the same compositional range are also shown in Figs. 4 and 7. The data indicate that there is an almost linear decrease from −450 μV/K at 10 m/o $InO_{1.5}$ to –180 μV/K at 40 m/o $InO_{1.5}$ (composition of the $k = 3$ superlattice). These values compare with a value of –350 μV/K for the solid solution ZnO containing 3 m/o $InO_{1.5}$.

VI. POTENTIAL BARRIER HEIGHT

The atomic structure of the superlattice interface and the reversal in polarity of the ZnO blocks on either side of the interface suggest that in addition to acting as a phonon barrier, there may also be an electron potential barrier at each InO_2 superlattice interface. Consequently, electrons with energies lower than the superlattice interface barrier height, ε_b, will have a high probability of being scattered, decreasing the overall conductivity, whereas those with excess energies will have a high probability of propagating over the barrier. (It has been proposed[5] that such "energy filtering" can also increase the Seebeck coefficient, S.). For a spatially homogeneous, degenerate n-type semiconductor, the Seebeck coefficient can be expressed in terms of the electron density of states at the Fermi level by the relationship[43]

$$S = \frac{1}{eT}\left[\frac{\int_0^\infty \tau(\varepsilon)g(\varepsilon)\varepsilon^2\left(-\frac{\partial f(\varepsilon)}{\partial \varepsilon}\right)d\varepsilon}{\int_0^\infty \tau(\varepsilon)g(\varepsilon)\varepsilon\left(-\frac{\partial f(\varepsilon)}{\partial \varepsilon}\right)d\varepsilon} - \mu\right], \qquad (1)$$

where e is the electronic charge, T is the absolute temperature, ε is the electron energy, $\tau(\varepsilon)$ is the relaxation time, $g(\varepsilon)$ is the density of states, $f(\varepsilon)$ is the Fermi distribution function, and μ is the Fermi energy. When superlattice interfaces are present, the electrons with energies below the superlattice interface potential barrier height ε_b are strongly scattered.

Because of the barriers, the equation for the Seebeck coefficient must be modified by replacing the lower limit of the integral with the potential barrier height, ε_b

$$S = \frac{1}{eT}\left[\frac{\int_{\varepsilon_b}^{\infty}\tau(\varepsilon)g(\varepsilon)\varepsilon^2\left(-\frac{\partial f(\varepsilon)}{\partial\varepsilon}\right)d\varepsilon}{\int_{\varepsilon_b}^{\infty}\tau(\varepsilon)g(\varepsilon)\varepsilon\left(-\frac{\partial f(\varepsilon)}{\partial\varepsilon}\right)d\varepsilon} - \mu\right]. \quad (2)$$

In the limit $\mu/k_BT \gg 1$, Kishimoto *et al.*[44] have shown that this equation can be approximated by

$$S = \frac{k_B}{e}\left[\eta^* + (1+\exp(\eta^*))\ln(1+\exp(-\eta^*))\right], \quad (3)$$

where $\eta^* = (\varepsilon_b - \mu)/k_BT$, and k_B is the Boltzmann constant. This, in turn, suggests that the variation in the Seebeck coefficient will be almost linear with the barrier height.

Using Eq. (3), the effective potential barrier heights $(\varepsilon_b - \mu)$ for the superlattice interfaces across the ZnO-In_2O_3 binary phase field can be estimated from the data for the Seebeck coefficient and electron conductivity.[17,27] This is shown, in Fig. 8, for the data at 800 °C as a function of indium oxide concentration. There is a strong dependence on composition and, equivalently, on the superlattice spacing $(k+1)d_{\{0002\}}$. In Fig. 8, the barrier height is superimposed on the same graph as the experimental data for the figure of merit, ZT

$$Z^*T = \frac{S^{*2}\sigma^*}{\kappa^*}T, \quad (4)$$

where the superscript * indicates measurements of the polycrystalline, bulk material. Comparison of the cross-plots in the figure indicates an inverse correlation between the two.

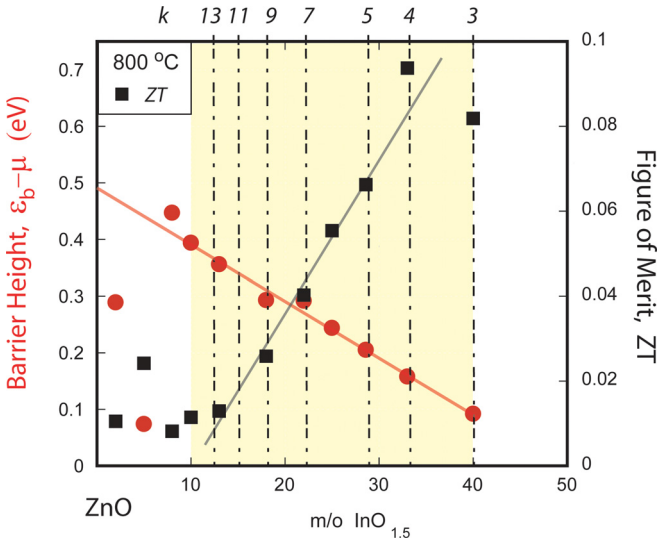

FIG. 8. Electron potential barrier height of $In_2O_3(ZnO)_k$ superlattice interfaces relative to the Fermi level estimated according to Eq. (3) with the input of Seebeck coefficients measured at 800 °C. Superimposed is the measured figure of merit ZT. The shaded region corresponds to the compositional range over which the natural superlattices form. The line through the barrier height data over the superlattice compositional range extrapolates to a barrier height of 0.49 eV.

In part, this is because the thermal conductivity (Fig. 4) is almost independent of composition and so the figure of merit is proportional to the $S^{*2}\sigma^*T$ product. Taken together with the increase in the Seebeck coefficient and the fact that the greatest change in the individual parameters with composition the conductivity, this would suggest that Z^*T is controlled by an interplay between barrier scattering of electrons and the barrier height determining the Seebeck coefficient. Accordingly, there should be an optimal effective barrier height that maximizes the power factor and therefore ZT, leading to the possibility of tuning both the power factor and ZT through composition control.

Assuming that the barrier height is the same for each InO_2 sheet, then in compositions where their spacing is sufficiently large, so that there are no interactions between the adjacent InO_2 sheets, the value of the barrier height can be extracted from the variation in the effective barrier height with the indium concentration. Thus, extrapolating the linear dependence of the barrier height in Fig. 8 to pure ZnO, corresponding to the limit of InO_2 sheets very far apart, the barrier height would have a value of 0.49 eV.

VII. DISCUSSION

Electrical and thermal transport in polycrystalline materials having a superlattice structure within the individual grains is complicated, and it is recognized that it cannot be fully understood on the basis of polycrystalline measurements alone. For instance, there are questions as to what extent can electrons transport in the ZnO blocks alone, whether and under what conditions can they cross the superlattice interfaces, and also whether they can also transport in the InO_2 sheets themselves as a parallel conduction path to conduction within the ZnO blocks. Furthermore, there is also the question as to what extent the boundaries between individual grains affect the measurements. Strictly speaking, answering these questions requires high-temperature studies of single crystals, but crystals do not exist. Nevertheless, some progress towards addressing these questions can be made by examining the systematic variation in properties with the superlattice spacing as is presented in this work. This is possible since the grain sizes are orders of magnitude larger (microns) than the superlattice spacings (nm), and consequently, the thermal resistance of the grain boundaries can be neglected.

We start with the observations reported in this work that the effective barrier height and electrical properties depend on the composition and hypothesize that it is likely that the barriers to electron transport are related to the InO_2 sheets themselves introducing conduction anisotropy. It could be argued that if the anisotropy is large, then electrons could flow between the sheets and not cross any potential barriers. But, as will be shown later, in a polycrystalline material, they must do so. For this reason, the focus in the following paragraphs is first on electrical transport across the InO_2 sheets in a single grain. It is proposed in this discussion that the barrier is associated with the band offset between InO_2 and ZnO although, as will also be discussed, this may be

modified by the polarization effects associated with the ZnO polarization.

Information regarding the band-gap of In_2O_3 is limited. There appears not to be a general consensus, but according to recent calculations, the band-gap has a value of 2.94 eV.[45] In contrast, there are numerous experimental data and *ab-initio* calculations indicating that the band-gap of ZnO is close to 3.4 eV.[46] Fortunately, ZnO is known to be an *n*-type semiconductor and our conductivity data confirm that indium doping of ZnO in the superlattice regime increases the *n*-type conductivity (Figs. 6 and 7). However, nothing is known about the conductivity of the InO_2 sheets themselves. Unless there are unidentified aliovalent impurities present, it is very likely that each is an intrinsic, albeit two-dimensional, semiconductor. As the Fermi levels of the InO_2 sheets and the ZnO blocks must coincide, this implies that the conduction band energy of the InO_2 sheets is higher than that of the ZnO, thereby providing an intrinsic barrier to electron transport. Assuming that the Fermi level is close to the conduction band in the ZnO blocks, this would give an estimate of the barrier height of 0.46 eV based on the difference in bandgaps. This estimate is consistent with the effective barrier height data in Fig. 8 when extrapolated to large values of k, namely, InO_2 sheets spaced far apart. The existence of a very narrow barrier due to the InO_2 sheets also provides a ready, albeit only qualitative, explanation for the unusual temperature independence of the electrical conductivity of the superlattice structures shown in Fig. 6.

This simple band-offset model does not, by itself, however, provide an explanation for one of the surprising results of this work: the effective barrier height varies with composition (Fig. 8), corresponding directly to the spacing of the InO_2 sheets. As each sheet, irrespective of their spacing, is chemically and structurally presumably the same and they are separated by blocks of ZnO, it is highly unlikely that the size of the block, i.e., the overall composition, can directly affect the effective barrier height. Furthermore, although it is possible that the Fermi energy in the blocks varies with their size, any such effect should already be included since the effective barrier height is the difference between the top of the barrier and the Fermi level. However, this band offset is also expected to be independent of material composition so an additional mechanism that affects the barrier height must be taken into account. We propose that the barrier height is affected by polarization effects associated with the fact that the InO_2 sheets are also crystallographically inversion interfaces in the superlattices.

As with other wurtzite compounds, such as GaN and AlN,[47] it is known that the direction of spontaneous polarization in ZnO is opposite to the direction of its c-axis. (By convention, the c-axis positive vector points from a Zn ion to an O ion and is perpendicular to the basal planes (0001) of the wurtzite structure.) Both experiments and *ab-initio* calculations indicate that the spontaneous polarization of ZnO has a value of about -0.05 C/m^2.[47,48] Thus, contrary to the common assumption that the polarization direction points from the cation to the anion, the direction of spontaneous polarization in ZnO is opposite. This direction of the spontaneous polarization, P_{SP}, is indicated in Fig. 9, an enlarged view of the atomic structure in the vicinity of the InO_2 sheets shown in Fig. 3.

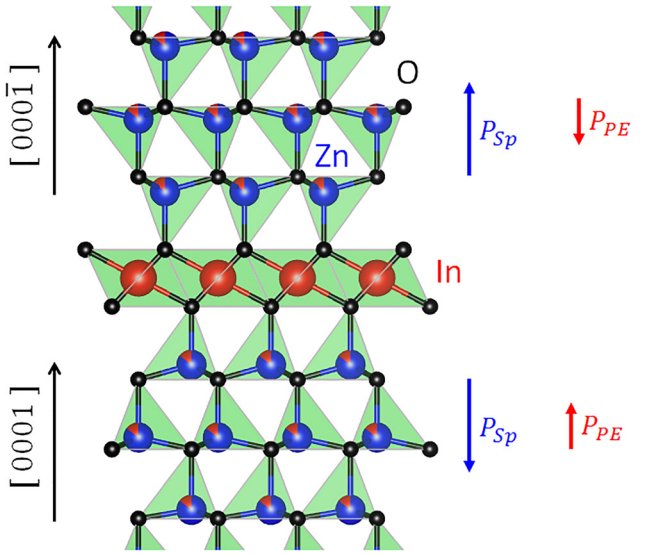

FIG. 9. Directions of the spontaneous, P_{Sp}, and strain-induced polarizations, P_{PE}, at the inversion boundary at the InO_2 sheet. Schematic. Drawn using Vesta software.

In addition to the spontaneous polarization inherent in any piezoelectric compound, it is also likely that there are strain-induced polarization effects, specifically associated with the elastic mismatch strain between the InO_2 sheets and the ZnO blocks. In the natural superlattice structure, the lattice correspondence can be expressed as an epitaxial relationship between the close packed planes in In_2O_3 and the basal planes in ZnO, namely, (111) In_2O_3//(0002) ZnO. Analysis of the superlattice X-ray diffraction patterns indicates that the a-axis and c-axis lattice parameters increase linearly with $InO_{1.5}$ concentrations as shown in Fig. 10. As a point of reference, in free-standing In_2O_3, the interatomic spacing in the close-packed {111} planes is 0.335 nm. This value happens to be the same as the interatomic spacing for the k = 3 superlattice (Fig. 10). If the embedded InO_2 sheets are assumed to remain pure InO_2, consistent with the EELS data, the lattice parameter data suggest that the InO_2 sheets are strain free at the k = 3 compositions but are under increasing in-plane compression as the indium concentration decreases towards ZnO. To balance the in-plane compression in the InO_2 sheets, the ZnO blocks are correspondingly under biaxial tension in the basal plane. In turn, this basal plane strain produces a piezoelectric polarization in the c-axis polar direction of the ZnO. The magnitude of the piezoelectric polarization is given by Ambacher *et al.*[49] for a strained film with a piezoelectric direction perpendicular to its substrate

$$P_{PE} = 2\frac{a - a_o}{a_o}\left[e_{31} - e_{33}\frac{C_{12}}{C_{33}}\right], \tag{5}$$

where the term outside the square bracket is the basal plane strain in the ZnO oxide and the square terms represent the conversion of a basal strain into a c-axis polarization. The piezoelectric strain coefficients e_{31} and e_{33} are those of ZnO.

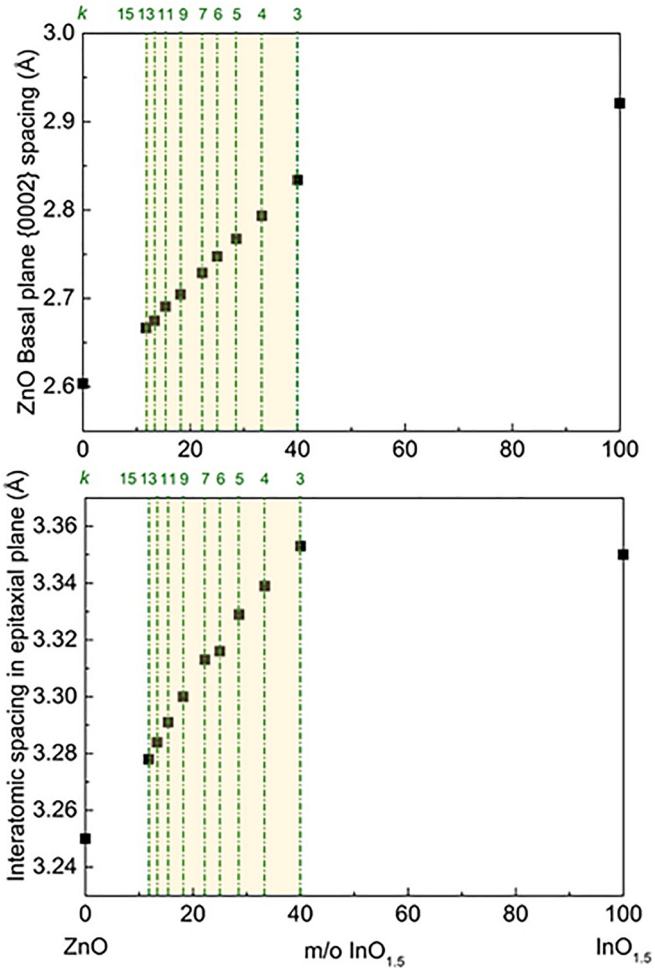

FIG. 10. The spacing between the ZnO planes along the c-axis and the in-plane spacing perpendicular to the c-axis with the concentration of $InO_{1.5}$ over the compositional range over which superlattices form. The linear increase implies that the in-plane spacing in the InO_2 sheets, embedded in the ZnO, generates an internal mismatch strain with the ZnO blocks. For comparison, the interatomic spacing in the close packed plane in In_2O_3 is 0.335 nm.

For pure ZnO, these are computed to have values of –0.51 and 1.21 C/m^2.[47] C_{12} and C_{33} are the stiffness coefficients of ZnO which are reported to have values of 1.211 and 2.109 $\times 10^{11}$ N m^{-2}, respectively. The term in the square brackets has a value of –1.145 for ZnO, meaning that compressive strain in the basal plane leads to a positive piezoelectric polarization in the ZnO along its c-axis. In our case, a and a_o are the interatomic spacings in the basal plane of the superlattice and strain-free ZnO containing In^{3+} ions in solid solution, respectively. This represents the in-plane, basal plane strain in the ZnO perpendicular to its c-axis. (Some of this strain is due to In^{3+} ions in solid solution, undeterminable from the X-ray data and some is due to strain due to epitaxial mismatch with the InO_2 sheet.) Notably, though, this piezoelectric polarization is opposite in sign to that of the spontaneous polarization. At the k = 3 composition, the piezoelectric contribution is zero as the interatomic spacing in the InO_2 sheets is the same as strain-free In_2O_3. However, the piezoelectric polarization increases with decreasing $InO_{1.5}$ concentrations as the interatomic spacing in the InO_2 sheets decreases and the mismatch increases. Consequently, in the compositional range over which superlattices form, increasing additions of $InO_{1.5}$ to ZnO introduces a higher density of InO_2 sheets, which because of the epitaxial relationship expands the ZnO a-axis, and introduces strain-induced (piezoelectric) polarization, P_{PE}, at the interfaces (Fig. 9). To summarize: because of the epitaxial relationship between the InO_2 sheets and the ZnO blocks, it is likely that there is a piezoelectric polarization at the InO_2 sheets which decreases with the increasing $InO_{1.5}$ concentrations consistent with the decrease in the barrier height shown in Fig. 8.

While the superlattice spacings in our material system are too small to enable direct measurements of the barrier height, it is noted that inversion twin boundaries also have been reported to occur in each grain in ZnO varistors when Sb_2O_3 is included in the compositional mix.[50,51] (The grain sizes in these varistor materials are typically several microns making the electrical measurements straightforward.) Voltage contrast imaging in the SEM, as well as micro-contact measurements on either side of these twin boundaries, indicates that there is a potential barrier when a voltage is applied across the inversion twin boundaries, where the Sb ions are located.[51] Based on the chemical and structural similarity between the In^{3+} and Sb^{3+} ions, we believe that these observations of a potential barrier in the Sb^{3+} doped ZnO are consistent with our suggestion that a barrier to transport across them exists at our natural superlattices.

As mentioned earlier, the materials we have studied were polycrystalline, with no detectable crystallographic texture, and all the measurements were made on these bulk materials not on single crystals. The superlattice created by the aligned InO_2 sheets and the associated potential distribution within individual grains are additional to the inherent electron mobility anisotropy between transport in the c-direction of the wurtzite ZnO and its basal plane. (The anisotropy for pure ZnO is reported to depend on temperature at temperatures below room temperature but negligible above.[52]) The thermoelectric figure of merit is related to the polycrystalline values of the properties in Eq. (4) and raises the question of how they are related to the single crystal values of the natural superlattice (Fig. 11). Some insight into this question comes from considering the polycrystalline averages of second-rank conductivity tensor properties. This was mathematically analyzed by Mityushov *et al.*[53] and subsequently validated by finite element calculations by Yang *et al.*[54] For second rank tensor conductivities, **A**, such as the electrical conductivity, thermal conductivity, and Seebeck coefficient, the tensor components are given by

$$A = \begin{pmatrix} a_x & 0 & 0 \\ 0 & a_x & 0 \\ 0 & 0 & a_z \end{pmatrix}. \tag{6}$$

The conductivity anisotropy can be expressed in terms of the ratio, $r = a_z/a_x$, the ratio of conductivity perpendicular to the InO_2 sheets divided by the conductivity parallel to them. According to Mityushov *et al.*, the third invariant of the conductivity has the value $a_m = \left(a_x^2 a_z\right)^{1/3}$. They also prove that the effective conductivity, a^*_{bulk}, of a bulk material containing randomly oriented grains, each with a single orientation of

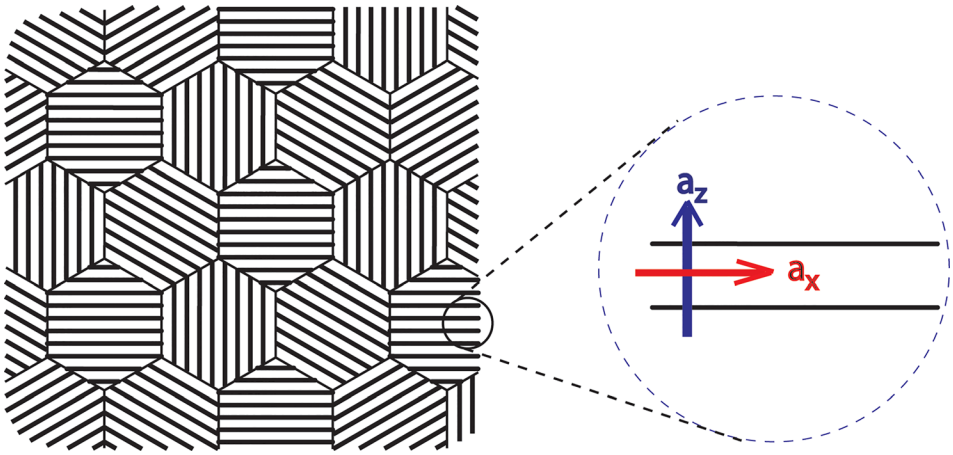

FIG. 11. Schematic diagram of a cross-section of a polycrystalline natural superlattice material in which each grain consists of an aligned superlattice structure of InO_2 sheets separated by blocks of ZnO. The conductivities parallel and perpendicular to the InO_2 sheets are defined as a_x and a_z, respectively. The diagram is exaggerated as the superlattice spacings are in nanometers, whereas the grain sizes are in microns.

aligned superlattices, and absent any texture, can be expressed as

$$a^*_{bulk}/a_m = \frac{r^{2/3}}{3} + \left[\frac{2}{3} - \frac{2}{9}\left(\frac{(r-1)^2}{r+2}\right)\right] r^{-1/3}. \quad (7)$$

One of the key features of this expression is that although the value of the conductivity of the bulk material depends on the conductivity anisotropy ratio, r, the single crystal conductivity anisotropy always affects the bulk conductivity of a polycrystalline material. In the context of this work, it means that the potential barrier associated with electron transport across the InO_2 sheets will always affect the measured electrical conductivity and the Seebeck coefficient of the polycrystalline bulk material under steady state conditions. So, even when the conductivity parallel to the sheets is many orders of magnitude larger than the conductivity perpendicular to the sheets, in which case the bulk conductivity tends to a value of $a^*_{bulk} \rightarrow 2a_x^{7/3}/(3a_z^{4/3})$, it is still affected by the anisotropy. Consequently, in a randomly oriented, polycrystalline bulk material, electrons must pass over barriers associated with the InO_2 sheets: while the electron flow may effectively short-circuit some of them, they cannot avoid them entirely. The same conclusion applies to the thermal conductivity as it is also a second-order rank tensor. Thus, even though the conductivity anisotropies as a function of composition remain to be determined in this material system, the overall thermoelectric properties of the polycrystalline material are affected by the presence of the InO_2 sheets and so they serve as effective barriers to electron and phonon transport in polycrystalline materials.

In summary, our work indicates that the InO_2 sheets in the $In_2O_3(ZnO)_k$ superlattices act to not only scatter phonons and decrease thermal conductivity but also alter the Seebeck coefficient and electrical conductivity. While energy filtering is beneficial in increasing the Seebeck effect, in this particular superlattice material system, the compositions with the lowest barrier heights exhibit the largest thermoelectric figure of merit presumably because of the larger electrical conductivities. Consequently, it is not possible in this system to simultaneously increase both electrical conductivity and Seebeck coefficients. However, not explored in this work is the possibility of modifying the electrical properties of the InO_2 sheets by isovalent substitution, for instance, using Fe^{3+} or Ga^{3+} to replace, in part, In^{3+} in the sheets.

In closing, we note that as a wide variety of natural superlattice oxides are known to exist and their compositions can be tailored by ionic substitutions according to established crystal chemical rules, we believe that this class of materials offers the opportunity for a new direction in seeking high-temperature thermoelectrics. For instance, since the original version of this paper was written, one of the authors has shown that both the Kapitza thermal resistance and the electron potential barrier of the polycrystalline $In_2O_3(ZnO)_9$ superlattice can be greatly increased by doping with Al^{3+}.[55] Small concentrations of Al^{3+} are known to substitute for In^{3+} and, based on their chemical bonding characteristics, are expected to enter the InO_2 sheets. What is especially intriguing about these recent findings is that the ionic substitution not only affects the potential barrier but also the thermal conductivity. The fact that similar natural superlattices have been reported to occur in the closely related ternary $ZnO\text{-}In_2O_3\text{-}Fe_2O_3$ and $ZnO\text{-}In_2O_3\text{-}Ga_2O_3$ systems[25,56–58] as well suggests that substitutional studies in these systems may also be of interest. They may also clarify the role of piezoelectric contributions, if any, to the potential barrier height. Furthermore, the flexibility afforded by ionic substitutional chemistry in other natural superlattices, such as in the $CaO(CaMnO_3)_k$, broadens the potential for natural superlattices as stable, high-temperature thermoelectrics.

ACKNOWLEDGMENTS

The authors wish to thank Takahiro Sato and Yoshihiro Ohtsu of the Hitachi High-Technologies Corporation, Electron Microscope Application Development Department, for their assistance with acquiring the high resolution STEM data. We are also grateful to Dr. Samuel Margueron for allowing us to use the data in Fig. 5.

[1]R. Venkatasubramanian *et al.*, "Thin-film thermoelectric devices with high room-temperature figures of merit," Nature **413**(6856), 597–602 (2001).
[2]A. Shakouri, "Recent developments in semiconductor thermoelectric physics and materials," Ann. Rev. Mater. Res. **41**, 399–431 (2011).
[3]E. S. Toberer, L. L. Baranowski, and C. Dames, "Advances in thermal conductivity," Annu. Rev. Mater. Res. **42**(1), 179–209 (2012).
[4]T. M. Tritt, "Thermoelectric phenomena, materials, and applications," Ann. Rev. Mater. Res. **41**, 433–448 (2011).

[5]D. Vashaee and A. Shakouri, "Improved thermoelectric power factor in metal-based superlattices," Phys. Rev. Lett. **92**(10), 106103 (2004).
[6]M. N. Luckyanova *et al.*, "Coherent phonon heat conduction in superlattices," Science **338**(6109), 936–939 (2012).
[7]R. M. Costescu *et al.*, "Ultra-low thermal conductivity in W/Al_2O_3 nanolaminates," Science **303**(5660), 989–990 (2004).
[8]C. Chiritescu *et al.*, "Ultralow thermal conductivity in disordered, layered WSe_2 crystals," Science **315**(5810), 351–353 (2007).
[9]Z. A. Sechrist *et al.*, "Optimization and structural characterization of W/Al_2O_3 nanolaminates grown using atomic layer deposition techniques," Chem. Mater. **17**(13), 3475–3485 (2005).
[10]P. J. Cannard and R. J. D. Tilley, "New intergrowth phases in the ZnO-In_2O_3 system," J. Solid State Chem. **73**(2), 418–426 (1988).
[11]M. A. McCoy, R. W. Grimes, and W. E. Lee, "Planar intergrowth structures in the ZnO-In_2O_3 system," Philos. Mag. A **76**(6), 1187–1201 (1997).
[12]M. Kazeoka *et al.*, "Improvement in thermoelectric properties of $(ZnO)_5In_2O_3$ through partial substitution of yttrium for indium," J. Mater. Res. **13**(3), 523–526 (1998).
[13]T. Moriga *et al.*, "Phase relationships and physical properties of homologous compounds in the zinc oxide-indium oxide system," J. Am. Ceram. Soc. **81**(5), 1310–1316 (1998).
[14]Y. Yan *et al.*, "Polytypoid structures in annealed In_2O_3-ZnO films," Appl. Phys. Lett. **73**(18), 2585–2587 (1998).
[15]Y. Masuda *et al.*, "Structure and thermoelectric transport properties of isoelectronically substituted $(ZnO)_5In_2O_3$," J. Solid State Chem. **150**(1), 221–227 (2000).
[16]H. W. Peng *et al.*, "Possible n-type carrier sources in $In_2O_3(ZnO)_k$," Chem. Mater. **24**(1), 106–114 (2012).
[17]X. Liang and D. R. Clarke, "Relation between thermoelectric properties and phase equilibria in the ZnO–In_2O_3 binary system," Acta Mater. **63**(0), 191–201 (2014).
[18]A. Baranovskiy and Y. Amouyal, "Dependence of electrical transport properties of $CaO(CaMnO3)_m$ ($m = 1, 2, 3, \infty$) thermoelectric oxides on lattice periodicity," J. Appl. Phys. **121**(6), 065103 (2017).
[19]C. Cardoso *et al.*, "Ab-initio calculations of the Ruddlesden-Popper phases $CaMnO_3$, $CaO(CaMnO_3)$ and $CaO(CaMnO_3)_2$," J. Phys.-Condens. Matter **20**(3), 035202 (2008).
[20]I. Terasaki, Y. Sasago, and K. Uchinokura, "Large thermoelectric power in $NaCo_2O_4$ single crystals," Phys. Rev. B **56**(20), R12685–R12687 (1997).
[21]Y. Y. Wang *et al.*, "Spin entropy as the likely source of enhanced thermopower in $Na_xCo_2O_4$," Nature **423**(6938), 425–428 (2003).
[22]C. Li *et al.*, "Structure analysis of new homologous compounds $Ga_2O_3(ZnO)_m$ ($m =$ integer) by high-resolution analytical transmission electron microscopy," Acta Crystallogr. Sect. B **55**(3), 355–362 (1999).
[23]G. B. Palmer and K. R. Poeppelmeier, "Phase relations, transparency and conductivity in Ga_2O_3-SnO_2-ZnO," Solid State Sci. **4**(3), 317–322 (2002).
[24]Y. Michiue, N. Kimizuka, and Y. Kanke, "Structure of $Ga_2O_3(ZnO)_6$: A member of the homologous series $Ga_2O_3(ZnO)_m$," Acta Crystallogr. Sect. B **64**(5), 521–526 (2008).
[25]N. Kimizuka, M. Isobe, and M. Nakamura, "Syntheses and single-crystal data of homologous compounds, $In_2O_3(ZnO)_m$ ($m = 3$, 4, and 5), $InGaO_3(ZnO)_3$, and $Ga_2O_3(ZnO)_m$ ($m = 7$, 8, 9, and 16) in the In_2O_3-$ZnGa_2O_4$-ZnO system," J. Solid State Chem. **116**(1), 170–178 (1995).
[26]X. Liang, M. Baram, and D. R. Clarke, "Thermal (Kapitza) resistance of interfaces in compositional dependent ZnO-In_2O_3 superlattices," Appl. Phys. Lett. **102**(22), 223903 (2013).
[27]X. Liang, *Structure and Thermoelectric Properties of ZnO Based Materials* (Harvard University, Cambridge, 2013).
[28]A. Yoshinari *et al.*, "Crystal and electronic band structures of homologous compounds $Zn_kIn_2O_{k+3}$ by Rietveld analysis and first-principle calculation," Mater. Res. Bull. **44**(2), 432–436 (2009).
[29]H. Schmid *et al.*, "Structural and elemental analysis of iron and indium doped zinc oxide by spectroscopic imaging in Cs-corrected STEM," Micron **43**(1), 49–56 (2012).
[30]H. Schmid, E. Okunishi, and W. Mader, "Defect structures in ZnO studied by high-resolution structural and spectroscopic imaging," Ultramicroscopy **127**, 76–84 (2013).
[31]M. Nakamura, N. Kimizuka, and T. Mohri, "The phaes relations in the In_2O_3-Ga_2ZnO_4-ZnO system at 1350 degree C," J. Solid State Chem. **93**(2), 298–315 (1991).
[32]C. Li *et al.*, "Relation between In ion ordering and crystal structure variation in homologous compounds $InMO_3(ZnO)_m$ (M=Al and In; m=integer)," Micron **31**(5), 543–550 (2000).
[33]M. A. McCoy, R. W. Grimes, and W. E. Lee, "Inversion domain boundaries in ZnO ceramics," J. Mater. Res. **11**(8), 2009–2019 (1996).
[34]K. Momma and F. Izumi, "VESTA 3 for three-dimensional visualization of crystal, volumetric and morphology data," J. Appl. Crystallogr. **44**, 1272–1276 (2011).
[35]ICDD, "PDF-4 + 2001 (Database)," (International Centre for Diffraction Data, Newtown Square, PA, 2011).
[36]F. Roder *et al.*, "Long range correlations in $In_2O_3(ZnO)_7$ investigated by DFT calculations and electron holography," Ultramicroscopy **110**, 400–410 (2010).
[37]S. M. Lee, D. G. Cahill, and R. Venkatasubramanian, Appl. Phys. Lett. **70**(22), 2957 (1997).
[38]D. G. Cahill, M. Katiyar, and J. R. Abelson, Phys. Rev. B **50**, 6077 (1994).
[39]A. Limarga and D. R. Clarke, "The grain size and temperature dependence of the thermal conductivity of polycrystalline, tetragonal yttria stabilized zirconia," Appl. Phys. Lett. **98**, 211906 (2011).
[40]S. Margueron *et al.*, "Optical and vibrational properties of $(ZnO)_kIn_2O_3$ natural superlattice nanostructures," J. Appl. Phys. **119**, 195103 (2016).
[41]P. Jood *et al.*, "Al-doped zinc oxide nanocomposites with enhanced thermoelectric properties," Nano Lett. **11**(10), 4337–4342 (2011).
[42]K. H. Kim *et al.*, "Microstructural and thermoelectric characteristics of zinc oxide-based thermoelectric materials fabricated using a spark plasma sintering process," J. Am. Ceram. Soc. **88**(3), 628–632 (2005).
[43]H. J. Goldsmid, *Introduction to Thermoelectricity*, Springer Series in Materials Science (Springer, Berlin, Heidelberg, 2010).
[44]K. Kishimoto, M. Tsukamoto, and T. Koyanagi, "Temperature dependence of the Seebeck coefficient and the potential barrier scattering of n-type PbTe films prepared on heated glass substrates by rf sputtering," J. Appl. Phys. **92**(9), 5331–5339 (2002).
[45]P. D. C. King *et al.*, "Band gap, electronic structure, and surface electron accumulation of cubic and rhombohedral In_2O_3," Phys. Rev. B **79**(20), 205211 (2009).
[46]H. Morkoc and U. Ozgur, *Zinc Oxide: Fundamentals, Materials and Devices* (Wiley, Weinheim, 2009).
[47]F. Bernardini, V. Fiorentini, and D. Vanderbilt, "Spontaneous polarization and piezoelectric constants of III-V nitrides," Phys. Rev. B **56**(16), R10024–R10027 (1997).
[48]A. Dalcorso *et al.*, "Ab-initio study of piezoelectricity and spontaneous polarization in ZnO," Phys. Rev. B **50**(15), 10715–10721 (1994).
[49]O. Ambacher *et al.*, "Two-dimensional electron gases induced by spontaneous and piezoelectric polarization charges in N- and Ga-face AlGaN/GaN heterostructures," J. Appl. Phys. **85**, 3222–3233 (1999).
[50]A. Recnik *et al.*, "Structure and chemistry of basal-plane inversion boundaries in antimony oxide-doped zinc oxide," J. Am. Ceram. Soc. **84**, 2657–2668 (2001).
[51]B. A. Haskell, S. J. Souri, and M. A. Helfand, "Varistor behavior at twin boundaries in ZnO," J. Am. Ceram. Soc. **82**(8), 2106–2110 (1999).
[52]P. Wagner and R. Helbig, "Hall-effect and anisotropy of electron-mobility in ZnO," J. Phys. Chem. Solids **35**(3), 327–335 (1974).
[53]E. A. Mityushov, R. A. Adamesku, and P. V. Gel'd, "Relation between kinetic properties of single crystals and of oriented polycrystalline materials," Inzhenero Fiz. Zh. **47**, 1052–1056 (1984).
[54]F. Yang *et al.*, "Effective thermal conductivity of polycrystalline materials with randomly oriented superlattice grains," J. Appl. Phys. **108**(3), 034310 (2010).
[55]X. Liang, "Remarkable enhancement in the Kapitza resistance and electron potential barrier of chemically modified $In_2O_3(ZnO)_9$ natural superlattice interfaces," Phys. Chem. Chem. Phys. **17**(44), 29655–29660 (2015).
[56]M. Nakamura, N. Kimizuka, and T. Mohri, "The phase relations in the In_2O_3-Fe_2ZnO_4-ZnO system at 1350 degree C," J. Solid State Chem. **86**(1), 16–40 (1990).
[57]N. Kimizuka *et al.*, "Syntheses and crystallographic data of the homologous compounds $InFeO_3(ZnO)_m$ ($m = 1$, 2, 3, 7, 11, 13, 15, and 19) and $Fe_2O_3(ZnO)_m$ ($m = 8$ and 9) in the In_2O_3-$ZnFe_2O_4$-ZnO system," J. Solid State Chem. **103**(2), 394–402 (1993).
[58]N. Uchida *et al.*, "High-resolution electron-microscopy of homologous compounds $InFeO_3(ZnO)_m$," J. Electron Microsc. **43**(3), 146–150 (1994).